JACS
JOURNAL OF THE AMERICAN CHEMICAL SOCIETY

Article

pubs.acs.org/JACS

Size-Controlled Synthesis of Porphyrinic Metal–Organic Framework and Functionalization for Targeted Photodynamic Therapy

Jihye Park,[†] Qin Jiang,[‡] Dawei Feng,[†] Lanqun Mao,*[,‡] and Hong-Cai Zhou*[,†]

[†]Department of Chemistry, Texas A&M University, College Station, Texas 77843-3255, United States

[‡]Beijing National Laboratory for Molecular Sciences, Key Laboratory of Analytical Chemistry for Living Biosystems, Institute of Chemistry, Chinese Academy of Sciences, Beijing, 100190, P. R. China

Supporting Information

ABSTRACT: The understanding of nanomaterials for targeted cancer therapy is of great importance as physical parameters of nanomaterials have been shown to be strong determinants that can promote cellular responses. However, there have been rare platforms that can vastly tune the core of nanoparticles at a molecular level despite various nanomaterials employed in such studies. Here we show targeted photodynamic therapy (PDT) with Zr(IV)-based porphyrinic metal–organic framework (MOF) nanoparticles. Through a bottom-up approach, the size of MOF nanoparticles was precisely tuned in a broad range with a designed functional motif, built upon selection of building blocks of the MOF. In particular, molecular properties of the porphyrinic linker are maintained in the MOF nanoparticles regardless of their sizes. Therefore, size-dependent cellular uptake and ensuing PDT allowed for screening of the optimal size of MOF nanoparticles for PDT while MOF nanoparticle formulation of the photosensitizer showed better PDT efficacy than that of its small molecule. Additionally, Zr_6 clusters in the MOF enabled an active targeting modality through postsynthetic modification, giving even more enhanced PDT efficacy. Together with our finding of size controllability covering a broad range in the nano regime, we envision that MOFs can be a promising nanoplatform by adopting advanced small molecule systems into the tunable framework with room for postsynthetic modification.

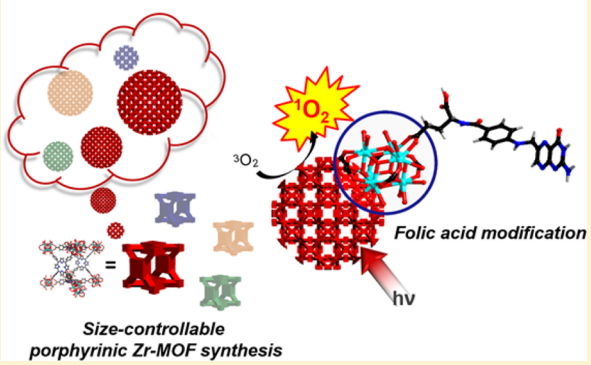

INTRODUCTION

Nanotechnology has shown great potential for cancer treatment due to the unique properties of nanomaterials, including optical, electrical, and magnetic behaviors. Meanwhile understanding the interactions between the nanomaterials and biological systems with respect to their size, shape, and surface chemistry is of significant importance when designing nanomaterials to improve the precision of cancer therapy.[1−4] Current nanomaterials in cancer therapy have evolved to improve specific accumulation at the tumor site with two major mechanisms: passive and active targeting. Passive targeting is often referred to as the enhanced permeability and retention (EPR) effect, while active targeting is achieved by coating targeting ligands onto the nanomaterials that can promote cellular uptake at the tumor sites.[5,6]

With conventional nanomaterials, however, achievement of such targeting modalities is often complex, because nanomaterials are usually employed as carriers of therapeutics or imaging agents, of which their inherent traits are hardly modifiable at a molecular level.[7] Recent studies reveal that physical parameters of nanomaterials have shown a strong correlation to cellular processes.[8−13] However, engineering of nanoparticles to carry a single variable for studying a targeted parameter remains a daunting challenge with formulations of conventional nanoparticles, because these often depend on more than one single factor.[14] Thus, such systems could disturb interpretation of the pure effects of the targeted parameter under controlled conditions, against other dependent variables. Therefore, it is of critical importance to integrate functionality into materials while having controllability of size and shape with no significant alteration of their designed physicochemical properties, as well as with a high degree of uniformity.[14−16]

As an emerging modality of cancer treatments, photodynamic therapy (PDT) has gained attention due to its minimally invasive nature and innate selectivity upon a localized irradiation at the tumor sites.[17,18] PDT requires a combination of light, a photosensitizer (PS), and tissue oxygen to generate cytotoxic singlet oxygen ($^1O_2$) that can damage tumors. Although porphyrin derivatives are widely employed photosensitizers in PDT, the effective delivery of porphyrinic molecules to the tumor sites still leaves much to be desired due to their hydrophobic nature.[19] Alternatively, nanomaterials have been involved as carriers for PDT therapeutics, but these examples often show limitations of

Received: January 1, 2016
Published: February 19, 2016

DOI: 10.1021/jacs.6b00007
J. Am. Chem. Soc. 2016, 138, 3518−3525

imprecise control of loading, increased toxicity, leaching, and instability.[15,20,21]

As an emerging class of porous materials, metal−organic frameworks (MOFs) have earned a significant amount of attention due to their superior design flexibility from their components of organic linkers and inorganic building blocks.[22,23] Despite broad interest in the synthesis of new MOFs, formulations of MOFs as nanomaterials have been relatively underdeveloped but a few synthetic methods (e.g., microwave, modulating chemical, spray-drying) have been applied.[42,44,53,54] Thus, expanding the study of nanomaterials with the design flexibility of MOFs at a molecular level can greatly diversify the core function of nanoparticles, broadening the scope of applications beyond the traditional use of their pores as carriers.[24−31] For instance, MOFs can integrate photosensitizers in periodic arrays, significantly reducing quenching of excited energy in a minimal volume, while allowing the accessibility of substrates due to their porous features.[32−34] In that regard, having MOFs as a base platform of nanomaterials can be advantageous due to their structural and chemical tunability via a bottom-up design. Here we show size-dependent targeted photodynamic therapy with porphyrinic Zr-MOF nanoparticles, PCN-224 (PCN stands for porous coordination network). The size-dependent cellular uptake and ensuing PDT were studied with various sizes of PCN-224 nanoparticles with an imaging and a therapeutic modality from the porphyrinic linker. In addition, further functionalization with folic acid (FA) onto the Zr_6 cluster in the MOF was also demonstrated, showing enhanced PDT efficacy owing to the active targeting of the modified MOF nanomaterial.

RESULTS AND DISCUSSION

Size-Controlled Synthesis of PCN-224 Nanoparticles.

In MOFs, each linker is spatially isolated by the framework, thus greatly preserving its molecular property regardless of dimensions. As a result, MOFs can be fully utilized as are small molecules, while their built-in properties are not affected by particle size.[35] We conceived that this feature would allow for maximization of passive targeting by screening optimal size of MOF nanoparticles for PDT. To investigate size-dependent targeted PDT, a Zr(IV)-based porphyrinic MOF was chosen as a model system to test our hypothesis. Zr(IV) is known for relatively good biocompatibility while its high valence allows strong electrostatic interaction with the carboxylate linkers in the MOF for the framework robustness.[36,37] Meanwhile, the photosensitizing ability as well as the emissive nature of the porphyrinic linker endows the theranostic modality of MOF, making this platform multifunctional. The concept of PDT was demonstrated by Lin and co-workers during the course of our study. Nonetheless, we believe that the investigation of size and other factors on a suitable platform (e.g., controlled morphology) would allow us to study a correlation between MOF nanoparticles and cellular uptake for maximization of therapeutic efficacy, addressing a gap in the literature. Of the many reported porphyrinic Zr-MOFs, PCN-224 was considered as a strong candidate due to its extraordinary chemical stability and nanoporous channels, allowing efficient diffusion of molecular oxygen.[38−40] Most importantly, the cubic space group of PCN-224 would allow for isotropic growth of crystals, enabling clearer size evaluation without having to carry dependent variables along with the size variation (e.g., aspect ratio, thickness in a rod, or a plate morphology) (Figure 1). Therefore, we chose PCN-224 as a model system for studying the particle size effect for targeted PDT.[38]

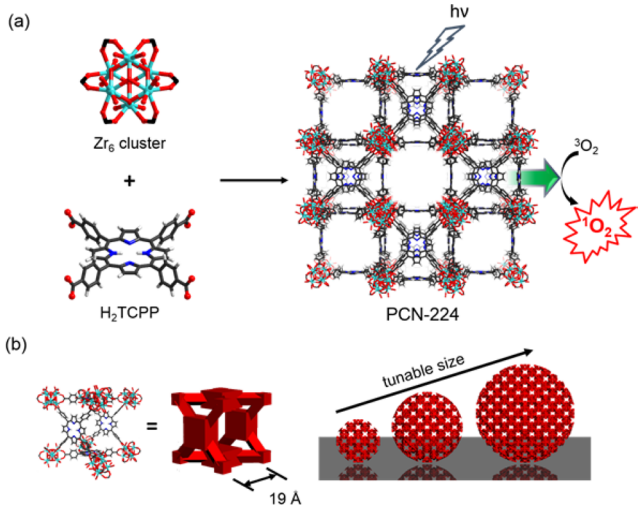

Figure 1. Illustration of PCN-224 structure. (a) 6-connected Zr_6 cluster ($Zr_6O_4(OH)_4(H_2O)_6(OH)_6(COO)_6$), tetratopic linker (tetrakis (4-carboxyphenyl)porphyrin (H_2TCPP)), and 3D nanoporous framework of PCN-224. (b) A cubic unit of PCN-224 and schematic illustration of spherical PCN-224 nanoparticles on the basis of construction of cubic units, yielding different sizes.

However, downsizing of PCN-224 from a millimeter scale to nanoscale upon varying the synthetic condition was not trivial due to the easy formation of unwanted phases. To overcome such difficulty, thermodynamic analysis was attempted along with the manipulation of synthetic conditions to tune the size of PCN-224 to nanoscale. In principle, MOF formation can be simplified as ligand substitution reactions on the metal clusters.[41,42] This simple coordination chemistry enables us to derive an equilibrium of MOF formation. In the specific example of PCN-224 synthesis, the equilibrium of the PCN-224 monomer (Zr_6 $(TCPP)_{1.5}$) formation can be simplified as eq 1 where excessive benzoic acid (BA) was employed as a competing reagent that is assumed to competitively coordinate to Zr_6 cluster, forming $Zr_6(BA)_{12}$. In this work, the PCN-224 monomer was defined as a soluble species with a negligible scattering contribution, where the formula of $Zr_6(TCPP)_{1.5}$ is derived from a repeating unit of PCN-224 (H_2O and extra OH^- in the Zr_6 cluster are ignored). Therefore, the formation of the PCN-224 monomer can be summarized as eq 2.

$$Zr_6(BA)_{12} + 1.5TCPP \overset{K}{\rightleftharpoons} Zr_6(TCPP)_{1.5} + 12BA \quad (1)$$

$$[\text{PCN-224}_{\text{monomer}}] = [Zr_6(TCPP)_{1.5}] = \frac{K \times [Zr_6(BA)_{12}] \times [TCPP]^{1.5}}{[BA]^{12}} \quad (2)$$

Ideally, manipulation of any factor in eq 2 would cause a change in the concentration of the PCN-224 monomer, which would eventually affect the particle size through the nucleation step.[43−46] However, our attempts to directly tune these factors (e.g., benzoic acid) from its synthetic condition of millimeter-sized single crystals failed to reduce the size to nanoscale, while giving phase impurity, presumably due to the dramatic change in the ratios between each reactant.

DOI: 10.1021/jacs.6b00007
J. Am. Chem. Soc. 2016, 138, 3518−3525

Thus, we embarked on downsizing PCN-224 by diluting the system to preserve the phase purity from unchanged stoichiometry between reactants, while aiming to create more MOF monomers, which would result in smaller particles (Supporting Information, SI, Sections S2–S4). Upon five times of dilution from its single crystal synthetic condition, PCN-224 nanoparticles with a size of ~90 nm, based on dynamic light scattering (DLS) in DMF, were achieved and this condition was established and denoted as a reference condition for the following investigation (Section S3). Then, we sought to realize a precise size control of the particles in the nano regime by utilizing different impact of size-tuning ability of each factor as analyzed. According to eq 2, for instance, the concentration of PCN-224 monomer is strongly dependent on the concentration of BA due to the high order of $[BA]^{12}$ in the equation, suggesting a significant impact of [BA] on the size of PCN-224 nanoparticles. Starting from the reference condition, when the amount of BA was varied with a ~200 mg interval from 2.2 to 3.3 g, the size of PCN-224 nanoparticles increased from 24 to 232 nm (Table S2). The tuning of the particle size in a narrower range was observed from variation of [TCPP] due to a lower order ($[TCPP]^{1.5}$) in the equation, making it a suitable variable for fine-tuning (Table S3). These results are also consistent with our thermodynamic analysis. For instance, according to eq 2, the increased amount of BA would result in decreased number of the PCN-224 monomer in the system, thus yielding larger nanoparticles. Similarly, varying the concentration of TCPP can also change the concentration of the monomer in an opposite trend to BA, which can also be predicted by eq 2. Therefore, adjustment of each factor in eq 2 allows fine-tuning of the size of PCN-224 nanoparticles. These results also suggest that understanding the size tunability of each factor holds great potential in providing design insights for nanomaterials that require such control in diverse future applications.

Among the variables, the set varied with the concentration of benzoic acid was chosen for detailed studies, due to an ease of variable control and a broad range of sizes. Powder X-ray diffraction (PXRD) data clearly show the pure phase of PCN-224 (Figure S2). To further confirm our hypothesis that the identity of MOF nanoparticles will not be altered by size variation, photophysical properties of the BA-varied set were tested by UV–vis and fluorescence spectroscopy. In absorption spectra, a slight red shift was observed as the particle size increased along with more scattering, as expected from typical observation in nanomaterials (Figure S4). Interestingly, their emission profiles, which are closely related to the photosensitization to generate $^1O_2$, show the same emission maxima (λ_{em} = 650 nm) for any size of samples, indicating the molecular level of design is well maintained regardless of their size (Figure 2a).

Having confirmed this unaltered molecular property of different sizes of PCN-224 nanoparticles, the stability of the framework in aqueous media was then examined. In Figure 2b, N_2 sorption of nanoparticles showed well maintained porosity compared to that of bulk crystalline PCN-224. Notably, after 24 h of water treatment at 37 °C, the porosity of PCN-224 nanoparticles was still preserved only with a slight decrease in N_2 uptake probably due to the inevitable destruction of the framework under aqueous condition (Figure 2b). PXRD data also confirmed that PCN-224 nanoparticles can retain their crystallinity in buffer (0.1 M HEPES, pH 7.4, 37 °C) for 2 days while gradually decreasing in crystallinity over 7 days (Figure 2c). In particular, PXRD data revealed that PCN-224 nanoparticles treated with cell culture medium, DMEM for 24 h maintained the crystallinity. These results indicate that PCN-224 nanoparticles would remain intact as the MOF until PDT treatment, considering typical cellular internalization and irradiation time for the treatment. To our surprise, PCN-224 nanoparticles can also be well dispersed in both DMF and H_2O in the absence of additional surfactant (Figure 2a inset). With most other conventional nanoparticles, surfactants are often required to prevent strong interparticle interaction for better dispersibility. Perhaps due to the 3D cubic grid-like porous structure of PCN-224 as well as its spherical morphology, it may provide tangential contact between particles, allowing minimal interaction on their surface. The ζ potential of PCN-224 nanoparticles of ~20 mV also supports their moderate dispersibility (Table 1). For instance, DLS data of PCN-224

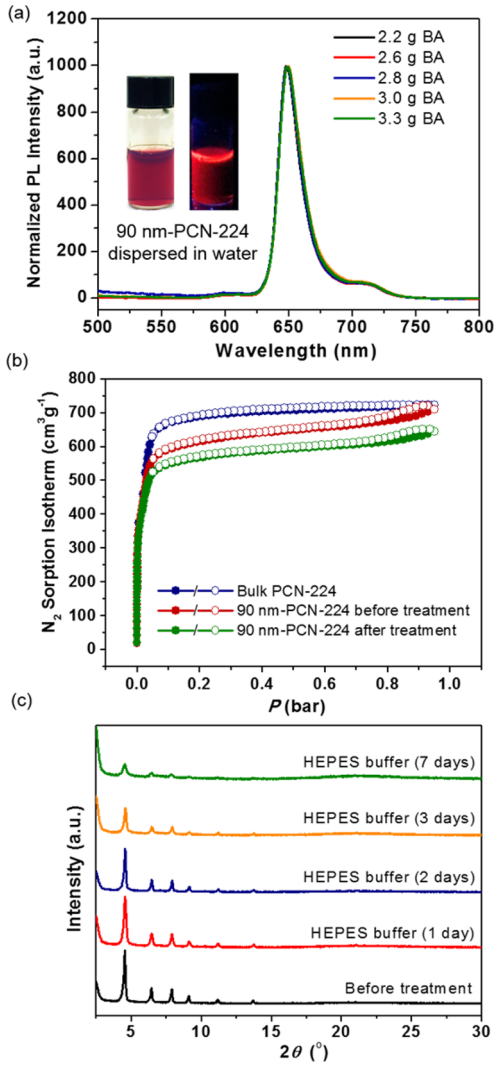

Figure 2. Characterization of PCN-224 nanoparticles. (a) Size-dependence of emission spectra (λ_{ex} = 420 nm). Inset: 90 nm-PCN-224 dispersed in water under (left) ambient light and (right) UV irradiation (λ = 365 nm), respectively. (b) N_2 adsorption isotherms of PCN-224 (bulk sample, 90 nm-PCN-224 before and after the water treatment (37 °C, 24 h). (c) Powder X-ray diffractions of PCN-224 nanoparticles after stability test (0.1 M HEPES, pH 7.4, 37 °C).

DOI: 10.1021/jacs.6b00007
J. Am. Chem. Soc. 2016, 138, 3518–3525

nanoparticles in water demonstrated good colloidal stability, showing no obvious aggregation for a week (Figure S10).

Table 1. Summary of Physicochemical Properties of PCN-224 Nanoparticles

label	BA (g)	TEM (nm)	D_h (nm)	PDI	ζ potential (mV)
30 nm	2.2	33 ± 4	65 ± 3	0.246	19.6 ± 6.41
60 nm	2.6	59 ± 5	114 ± 3	0.067	25.3 ± 6.27
90 nm	2.8	91 ± 8	137 ± 2	0.053	19.8 ± 7.15
140 nm	3.0	144 ± 7	197 ± 1	0.035	22.7 ± 5.92
190 nm	3.3	189 ± 11	255 ± 2	0.025	20.7 ± 5.59

Passive Targeting: Particle Size-Dependent Cellular Uptake and PDT. Although the effect of physical dimension of some other nanoparticles (i.e., gold nanoparticles, carbon nanotubes) for cellular uptake has been studied, it has been known that their correlations are also significantly affected by the composition of the nanomaterials.[14] Considering only a rare example can be referred as a study of the size-related cellular response with MOF nanomaterials,[47] PCN-224 model platform, covering a broad range in interest of biological studies, can provide important design insight for future study in MOF size-cell interaction. To determine the size-dependent cellular response, five size fractions, ranging from 30 to 190 nm, based on transmission electron microscopy (TEM) results, were applied to HeLa (human cervical cancer) cells (Table 1 and Figure 3a). Quantitative analysis of uptake of the nanoparticles was achieved using inductively coupled plasma mass spectrometry (ICP-MS) upon cell digestion. To begin, time-dependent cellular uptake of PCN-224 nanoparticles was studied to obtain insight for kinetics of endocytosis. The cellular uptake showed a plateau around 12 h for each fraction (Figure 3b). Dose-dependent uptake of PCN-224, ranging from 0.5 to 40 μM (TCPP equiv), was also carried out. Interestingly, ICP results indicate that different amount of Zr entered into the cells, suggesting the different sizes of particles indeed resulted in different cellular responses (Figure 3c). Notably, 90 nm-PCN-224 showed the highest amount of Zr uptake in cells which also suggests the greatest uptake of TCPP by MOF structure, among other sizes (Figure 4a and Section S10).

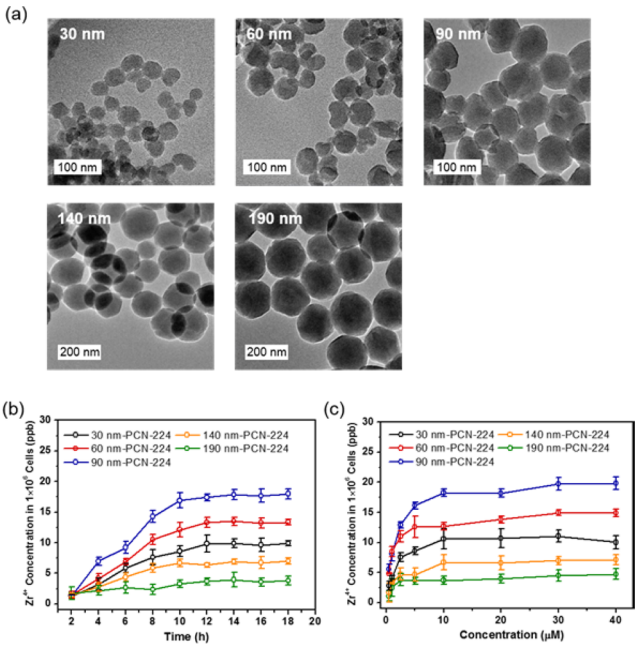

Figure 3. (a) TEM images of PCN-224 nanoparticles of 30, 60, 90, 140, and 190 nm. (b) Cellular uptake of PCN-224 samples with different sizes at various incubation time. Concentration = 20 μM. (c) Cellular uptake of different sized PCN-224 nanoparticles at various concentrations. Incubation time = 24 h. Data are based on ICP analysis of the Zr concentration internalized into HeLa cells. Data are means ± s.d. (N = 3).

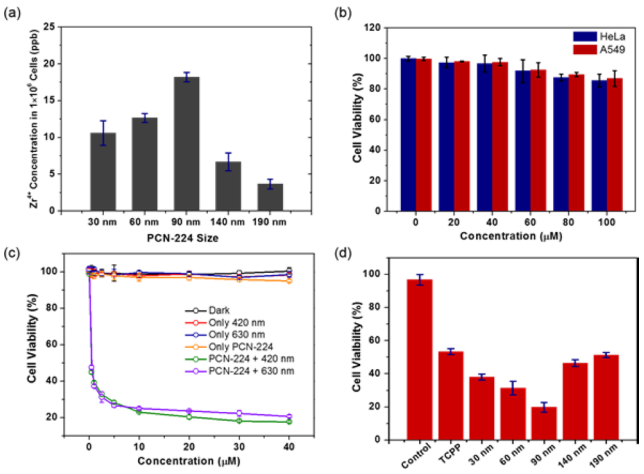

Figure 4. (a) Size-dependent cellular uptake of PCN-224 nanoparticles. Incubation time = 24 h. (b) Cytotoxicity of 90 nm-PCN-224 in HeLa and A549 cells at various concentrations for 48 h. (c) Control experiments of cytotoxicity in HeLa cells upon light irradiation of 420 and 630 nm in the absence and presence of 90 nm-PCN-224. Irradiation time = 30 min. (d) Comparison of PDT efficacy between different sized PCN-224 nanoparticles and free TCPP molecules. Data are means ± s.d. (N = 3).

Having examined size-dependent cellular uptake of PCN-224 nanoparticles, PDT efficacy of the five size fractions, each at 20 μM, were tested for HeLa cells under irradiation at Soret band (420 nm). Among these five fractions, 90 nm-PCN-224 showed the best PDT efficacy of 81%, while 190 nm-PCN-224 gave the lowest efficacy of 49% in agreement with the results of cellular uptake (Figure 4d). Markedly, free photosensitizer (TCPP linker only) showed only 47% in PDT efficacy at the same concentration, which further confirms our hypothesis that MOF nanoparticle formulation and the size screening can optimize the performance of the given photosensitizer. Interestingly, the PDT efficacy does not show much correlation with the number of nanoparticles inside the cells where we converted Zr content to the number of particles (Section S10). Rather, 90 nm-PCN-224 with a moderate number of particles internalized shows the greatest PDT efficacy as a result of the highest Zr/TCPP uptake (Figure 4d) while showing no evident toxicity of the material itself even at high concentration after 48 h incubation (viability of ~90% at 100 μM) (Figure 4b). These results clearly show a strong correlation between PDT efficacy and the TCPP concentration in the cells, rather than the number of particles. Such correlation, therefore, indicates that TCPP linkers in PCN-224 nanoparticles are fully utilized regardless of the particle size, as are small molecules, resulting from the 3D nanoporous structure of PCN-224 while preference for internalization was determined by the size of MOF nano-

DOI: 10.1021/jacs.6b00007
J. Am. Chem. Soc. 2016, 138, 3518−3525

particle. It is important to note that these results address the need for insights in the design/selection of MOFs, because the density of desired function in the framework is proportional to the size, while the size parameter is another determinant for optimizing the dynamics between materials and cells.

Because TCPP can absorb the light at Q bands other than its Soret band, we further investigated the PDT efficacy of the size optimized PCN-224 nanoparticles (90 nm) under irradiation at 630 nm, which would provide better tissue penetration in practice. Although the irradiation at 420 nm showed slightly better $^1O_2$ generation than at 630 nm due to the strong absorption of the Soret band in singlet oxygen generation study (Figure S14), PDT efficacy of 90 nm PCN-224 under 630 nm irradiation could reach as high as ~80%, which is almost the same as the efficacy under 420 nm irradiation (Figure 4c). Presumably due to the highly dense assembly of TCPP in PCN-224, while the framework prevents the aggregation of photosensitizers, O_2 molecules in cells might have sufficient contact with surrounding photosensitizers. Consequently, the weaker absorption of TCPP at 630 nm irradiation may be compensated by sufficient interaction between O_2 and photosensitizers inside of PCN-224 nanoparticles, resulting in similar efficacy (Figure S14). Utilizing red emission of TCPP, we further tested PCN-224 for cell imaging through confocal laser scanning microscopy (CLSM) (Figure S11). In addition, the subcellular localization of PCN-224 in HeLa cells was confirmed with fluorescent staining. Notably, the red fluorescence of PCN-224 matches well with the green fluorescence from Lyso Tracker and Mito Tracker, while showing negligible overlap between PCN-224 and nucleus, indicating the PCN-224 nanoparticles are mostly localized in the cytoplasm (Figure 5).

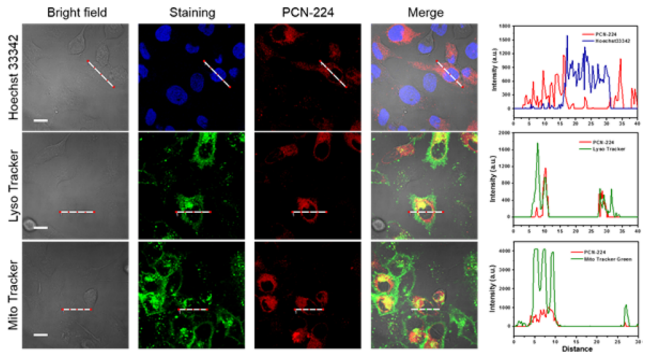

Figure 5. Subcellular localization of PCN-224 nanoparticles by staining with organelle markers, Hoechst 33342, Lyso Tracker, and Mito Tracker green.

Active Targeting: Folic Acid Modification on PCN-224 Nanoparticles. Folate is a commonly used ligand for targeting folate receptor (FAR) abundant tumor cells, including ovarian tumors, to enhance the delivery of nanoparticles/drugs.[48,49] Therefore, we further sought to build an active targeting modality in our platform through postsynthetic folic acid (FA) modification on the surface of 90 nm-PCN-224. Because there are available binding sites on the Zr_6 cluster in PCN-224, the carboxylate end of folate could be attached to Zr_6 clusters by coordination (Figure 6a).[50] However, as previous results suggest that the size of nanoparticles will also affect the uptake, the degree of FA functionalization was designed to bear a minimal size expansion to prepare comparable sizes. A series of FA modified 90 nm-PCN-224 was prepared by reaction with different stoichiometries of 1/8, 1/4, and 1/2 equiv of FA to the available Zr binding sites. The size of samples was confirmed by TEM and DLS, which showed the modification extent, not involving drastic changes in size and surface charge (Figure S20 and Table S7). Also, the characteristic absorption band of FA confirmed the different degree of FA functionalization as well as quantification of actual FA loading of each sample (Figure S19 and Table S6). $^1O_2$ generating ability of PCN-224 nanoparticles after the FA modification remains almost the same as pristine PCN-224 nanoparticles, providing a good control to evaluate the influence of FA modification (Figure S21). In order to test the active targeting upon FA modification, the PDT efficacy of samples was tested with HeLa cells, known for FAR abundant cell line.[51] As a result, 1/4FA-PCN-224 showed the most potency: more than 90% of PDT efficacy, which is an enhancement from unmodified PCN-224 under the same condition (Figure 6b). Although any degree of FA modification provided an enhancement from the unmodified sample, the lesser enhancement from 1/8FA-PCN-224 may result from insufficient FA density than that of 1/4FA-PCN-224, whereas 1/2FA-PCN-224 showed the least enhancement perhaps due to the size expansion (Figure 6b). Overall, this improvement in PDT efficacy shows the great potential of this system of which the maximization of the desired function can be achieved through optimizations of both physical and chemical properties of the MOF nanoplatform.

To further confirm the effect of active targeting, both FA modified and unmodified 90 nm-PCN-224 were applied to FAR-negative cell line, A549 as a control experiment. Interestingly, FA functionalized PCN-224 showed no apparent advantages over unmodified nanoparticles both in uptake and ensuing PDT efficacy, rather it showed even less merit (Figure 6c,e). Likely due to different size preferences for permeability of the particles in A549 cells, a slight increase in size of PCN-224 upon FA modification showed rather negative impacts on the uptake in FAR negative A549 cells (Figure 6c–f). In parallel, a competition assay was implemented with 1/4FA-PCN-224 in the presence of an excess amount of free FA as a competing ligand for folate receptor.[52] Indeed, HeLa cells treated with the excess free FA (1 mM) showed much weaker fluorescence in confocal microscopy images, indicating functionalized FA on the MOF was involved in the uptake event through receptor-mediated endocytosis (Figure 6g).

CONCLUSIONS

Through thermodynamic analysis, the size of PCN-224 nanoparticles was successfully tuned to a range that is of interest to biological studies (30–190 nm). Our hypothesis is successfully proved by preferential cellular uptake of 90 nm-PCN-224 and its remarkable PDT efficacy over other sizes, including free TCPP linkers. These results clearly demonstrate the fabrication of photosensitizer as MOF nanoparticles followed by the optimization of their size parameter indeed play a critical role for improving cellular response. Together with our findings in size-controllable synthesis of MOF nanoparticles, the PCN-224 nanoplatform demonstrates active targeting modality for further enhancement of PDT efficacy, of which the enhancement was obtained by postsynthetic FA modification onto Zr_6 cluster. Meanwhile, the potential of

DOI: 10.1021/jacs.6b00007
J. Am. Chem. Soc. 2016, 138, 3518–3525

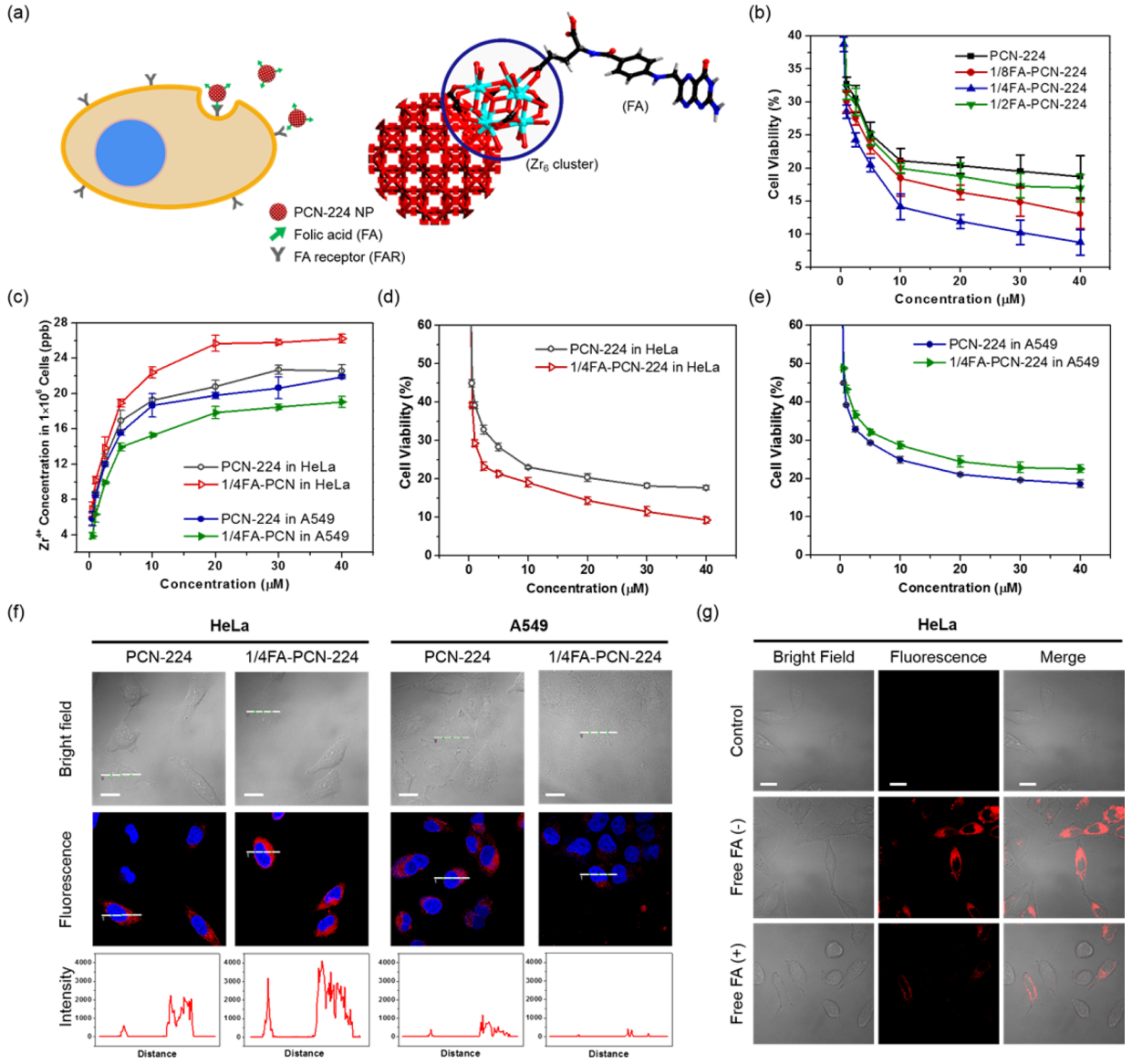

Figure 6. In vitro PDT study of FA functionalized 90 nm-PCN-224. (a) Scheme of FA functionalized PCN-224 nanoparticle and proposed internalization. (b) In vitro PDT efficacy of FA functionalized (FA equivalent of 0, 1/8, 1/4, 1/2) 90 nm-PCN-224 at various concentrations in HeLa cells. Irradiation at 420 nm for 30 min for PDT. (c) ICP analysis of cellular uptake of unfunctionalized and FA functionalized 90 nm-PCN-224 at various concentrations in HeLa and A549 cells. Incubation time =24 h. (d,e) Comparison of in vitro PDT efficacy of pristine PCN-224 and 1/4FA-PCN-224 in (d) HeLa cells and (e) A549 cells. (f) CLSM images of HeLa and A549 cells incubated with pristine PCN-224 and 1/4FA-PCN-224 samples. Red channel images were obtained from pristine or FA functionalized PCN-224. The blue channel images were obtained from Hoechst 33342 (nucleus). Concentration =20 μM. Incubation time =60 min. Scale bars =20 μm. (g) CLSM images of HeLa cells without any treatment (top row); treated with 1/4FA-PCN-224 (middle row); coincubated with excess amount of free FA (1 mM) and 1/4FA-PCN-224 (bottom row). Concentration =20 μM. Incubation time =60 min. Scale bars =20 μm. Data are means ± s.d. (N = 3).

theranostic modality was demonstrated from the porphyrinic linker in the MOF in cancer cell model. Having confirmed the preserved molecular properties of the incorporated linker, invariable to MOF sizes, we envision that combination of the synthetic tunability of MOF on the molecular scale and its size controllability can create useful tools for specific needs in desired applications through chemical, physical, and structural design of MOF nanoplatform.

EXPERIMENTAL SECTION

Single Crystalline PCN-224. 5,10, 15, 20-Tetrakis (4-carboxyphenyl)porphyrin (H_2TCPP) (10 mg, 0.013 mmol), zirconyl chloride octahydrate ($ZrOCl_2 \cdot 8H_2O$) (30 mg, 0.093 mmol), and benzoic acid (BA) (300 mg, 2.4 mmol) in 2 mL of *N,N*-Dimethylformamide (DMF) were ultrasonically dissolved in a Pyrex vial. The reaction mixture was heated in the 120 °C oven for 24 h. After being cooled to room temperature, dark purple crystals were harvested by filtration.

90 nm-PCN-224 (Reference Condition). H_2TCPP (100 mg, 0.13 mmol), $ZrOCl_2 \cdot 8H_2O$ (300 mg, 0.93 mmol), and benzoic acid (2.8 g, 23 mmol) were dissolved in 100 mL of DMF in a 250 mL round-bottom flask and the mixture was stirred (300 rpm) at 90 °C for 5 h. After the reaction is done, PCN-224 nanoparticles were collected by centrifugation (15 000 rpm, 30 min) followed by washing with fresh DMF for 3 times. The resulting PCN-224 nanoparticles were suspended in DMF for further characterization and analysis.

Detailed discussion and methods can be found in the SI.

DOI: 10.1021/jacs.6b00007
J. Am. Chem. Soc. 2016, 138, 3518−3525

■ ASSOCIATED CONTENT

Supporting Information

The Supporting Information is available free of charge on the ACS Publications website at DOI: 10.1021/jacs.6b00007.

Full details of sample preparation and characterization results (PDF)

■ AUTHOR INFORMATION

Corresponding Authors

*zhou@mail.chem.tamu.edu

*lqmao@iccas.ac.cn

Notes

The authors declare no competing financial interest.

■ ACKNOWLEDGMENTS

The syntheses of MOFs and their characterizations were supported as part of the Center for Gas Separations Relevant to Clean Energy Technologies, an Energy Frontier Research Center funded by the U.S. Department of Energy, Office of Science, and Office of Basic Energy Sciences under Award Number DE-SC0001015. H.-C.Z. was supported by Texas A&M University. Also, use of the Texas A&M University Laboratory for Synthetic-Biologic Interactions is acknowledged. The authors gratefully acknowledge Dr. Zhangwen Wei for assistance with simulating structures and others for helpful discussion.

■ REFERENCES

(1) Ferrari, M. *Nat. Rev. Cancer* **2005**, *5*, 161−171.

(2) Barreto, J. A.; O'Malley, W.; Kubeil, M.; Graham, B.; Stephan, H.; Spiccia, L. *Adv. Mater.* **2011**, *23*, H18−40.

(3) Lammers, T.; Aime, S.; Hennink, W. E.; Storm, G.; Kiessling, F. *Acc. Chem. Res.* **2011**, *44*, 1029−1038.

(4) Schroeder, A.; Heller, D. A.; Winslow, M. M.; Dahlman, J. E.; Pratt, G. W.; Langer, R.; Jacks, T.; Anderson, D. G. *Nat. Rev. Cancer* **2011**, *12*, 39−50.

(5) Davis, M. E.; Chen, Z.; Shin, D. M. *Nat. Rev. Drug Discovery* **2008**, *7*, 771−782.

(6) Peer, D.; Karp, J. M.; Hong, S.; FaroKhzad, O. C.; Margalit, R.; Langer, R. *Nat. Nanotechnol.* **2007**, *2*, 751−760.

(7) Wang, A. Z.; Langer, R.; Farokhzad, O. C. *Annu. Rev. Med.* **2012**, *63*, 185−198.

(8) Jiang, W.; Kim, B. Y. S.; Rutka, J. T.; Chan, W. C. W. *Nat. Nanotechnol.* **2008**, *3*, 145−150.

(9) Jin, H.; Heller, D. A.; Sharma, R.; Strano, M. S. *ACS Nano* **2009**, *3*, 149−158.

(10) Lu, F.; Wu, S.-H.; Hung, Y.; Mou, C.-Y. *Small* **2009**, *5*, 1408−1413.

(11) Nel, A. E.; Maedler, L.; Velegol, D.; Xia, T.; Hoek, E. M. V.; Somasundaran, P.; Klaessig, F.; Castranova, V.; Thompson, M. *Nat. Mater.* **2009**, *8*, 543−557.

(12) Sykes, E. A.; Chen, J.; Zheng, G.; Chan, W. C. W. *ACS Nano* **2014**, *8*, 5696−5706.

(13) Zhang, S.; Li, J.; Lykotrafitis, G.; Bao, G.; Suresh, S. *Adv. Mater.* **2009**, *21*, 419−424.

(14) Albanese, A.; Tang, P. S.; Chan, W. C. W. *Annu. Rev. Biomed. Eng.* **2012**, *14*, 1−16.

(15) Alkilany, A. M.; Murphy, C. J. *J. Nanopart. Res.* **2010**, *12*, 2313−2333.

(16) Sailor, M. J.; Park, J.-H. *Adv. Mater.* **2012**, *24*, 3779−3802.

(17) Chatterjee, D. K.; Fong, L. S.; Zhang, Y. *Adv. Drug Delivery Rev.* **2008**, *60*, 1627−1637.

(18) Dolmans, D. E. J. G. J.; Fukumura, D.; Jain, R. K. *Nat. Rev. Cancer* **2003**, *3*, 380−387.

(19) Konan, Y. N.; Gurny, R.; Allémann, E. *J. Photochem. Photobiol., B* **2002**, *66*, 89−106.

(20) Alkilany, A. M.; Nagaria, P. K.; Hexel, C. R.; Shaw, T. J.; Murphy, C. J.; Wyatt, M. D. *Small* **2009**, *5*, 701−708.

(21) Bechet, D.; Couleaud, P.; Frochot, C.; Viriot, M.-L.; Guillemin, F.; Barberi-Heyob, M. *Trends Biotechnol.* **2008**, *26*, 612−621.

(22) Furukawa, H.; Cordova, K. E.; O'Keeffe, M.; Yaghi, O. M. *Science* **2013**, *341*, 1230444.

(23) Zhou, H.-C.; Long, J. R.; Yaghi, O. M. *Chem. Rev.* **2012**, *112*, 673−674.

(24) Allendorf, M. D.; Bauer, C. A.; Bhakta, R. K.; Houk, R. J. T. *Chem. Soc. Rev.* **2009**, *38*, 1330−1352.

(25) He, C.; Liu, D.; Lin, W. *Chem. Rev.* **2015**, *115*, 11079−11108.

(26) Horcajada, P.; Chalati, T.; Serre, C.; Gillet, B.; Sebrie, C.; Baati, T.; Eubank, J. F.; Heurtaux, D.; Clayette, P.; Kreuz, C.; Chang, J.-S.; Hwang, Y. K.; Marsaud, V.; Bories, P.-N.; Cynober, L.; Gil, S.; Ferey, G.; Couvreur, P.; Gref, R. *Nat. Mater.* **2010**, *9*, 172−178.

(27) Horcajada, P.; Gref, R.; Baati, T.; Allan, P. K.; Maurin, G.; Couvreur, P.; Ferey, G.; Morris, R. E.; Serre, C. *Chem. Rev.* **2012**, *112*, 1232−1268.

(28) Matsuda, R.; Kitaura, R.; Kitagawa, S.; Kubota, Y.; Belosludov, R. V.; Kobayashi, T. C.; Sakamoto, H.; Chiba, T.; Takata, M.; Kawazoe, Y.; Mita, Y. *Nature* **2005**, *436*, 238−241.

(29) Moon, H. R.; Lim, D.-W; Suh, M. P. *Chem. Soc. Rev.* **2013**, *42*, 1807−1824.

(30) Sindoro, M.; Yanai, N.; Jee, A.-Y.; Granick, S. *Acc. Chem. Res.* **2014**, *47*, 459−469.

(31) Zhang, L.; Lei, J.; Ma, F.; Ling, P.; Liu, J.; Ju, H. *Chem. Commun.* **2015**, *51*, 10831−10834.

(32) Lee, C. Y.; Farha, O. K.; Hong, B. J.; Sarjeant, A. A.; Nguyen, S. T.; Hupp, J. T. *J. Am. Chem. Soc.* **2011**, *133*, 15858−15861.

(33) Lu, K.; He, C.; Lin, W. *J. Am. Chem. Soc.* **2014**, *136*, 16712−16715.

(34) Zhang, T.; Lin, W. *Chem. Soc. Rev.* **2014**, *43*, 5982−5993.

(35) Yoon, M.; Srirambalaji, R.; Kim, K. *Chem. Rev.* **2012**, *112*, 1196−1231.

(36) Cavka, J. H.; Jakobsen, S.; Olsbye, U.; Guillou, N.; Lamberti, C.; Bordiga, S.; Lillerud, K. P. *J. Am. Chem. Soc.* **2008**, *130*, 13850−13851.

(37) Huan, Z. G.; Leeflang, M. A.; Zhou, J.; Fratila-Apachitei, L. E.; Duszczyk, J. *J. Mater. Sci.: Mater. Med.* **2010**, *21*, 2623−2635.

(38) Feng, D.; Chung, W.-C.; Wei, Z.; Gu, Z.-Y.; Jiang, H.-L.; Chen, Y.-P.; Darensbourg, D. J.; Zhou, H.-C. *J. Am. Chem. Soc.* **2013**, *135*, 17105−17110.

(39) Feng, D.; Gu, Z.-Y.; Li, J.-R.; Jiang, H.-L.; Wei, Z.; Zhou, H.-C. *Angew. Chem., Int. Ed.* **2012**, *51*, 10307−10310.

(40) Morris, W.; Volosskiy, B.; Demir, S.; Gándara, F.; McGrier, P. L.; Furukawa, H.; Cascio, D.; Stoddart, J. F.; Yaghi, O. M. *Inorg. Chem.* **2012**, *51*, 6443−6445.

(41) Feng, D.; Wang, K.; Wei, Z.; Chen, Y.-P.; Simon, C. M.; Arvapally, R. K.; Martin, R. L.; Bosch, M.; Liu, T.-F.; Fordham, S.; Yuan, D.; Omary, M. A.; Haranczyk, M.; Smit, B.; Zhou, H.-C. *Nat. Commun.* **2014**, *5*, 5723.

(42) Tsuruoka, T.; Furukawa, S.; Takashima, Y.; Yoshida, K.; Isoda, S.; Kitagawa, S. *Angew. Chem., Int. Ed.* **2009**, *48*, 4739−4743.

(43) Patterson, J. P.; Abellan, P.; Denny, M. S.; Park, C.; Browning, N. D.; Cohen, S. M.; Evans, J. E.; Gianneschi, N. C. *J. Am. Chem. Soc.* **2015**, *137*, 7322−7328.

(44) Schaate, A.; Roy, P.; Godt, A.; Lippke, J.; Waltz, F.; Wiebcke, M.; Behrens, P. *Chem. - Eur. J.* **2011**, *17*, 6643−6651.

(45) Thanh, N. T. K.; Maclean, N.; Mahiddine, S. *Chem. Rev.* **2014**, *114*, 7610−7630.

(46) Zahn, G.; Zerner, P.; Lippke, J.; Kempf, F. L.; Lilienthal, S.; Schroder, C. A.; Schneider, A. M.; Behrens, P. *CrystEngComm* **2014**, *16*, 9198−9207.

(47) Morris, W.; Briley, W. E.; Auyeung, E.; Cabezas, M. D.; Mirkin, C. A. *J. Am. Chem. Soc.* **2014**, *136*, 7261−7264.

(48) Low, P. S.; Kularatne, S. A. *Curr. Opin. Chem. Biol.* **2009**, *13*, 256−262.

(49) Xia, W.; Low, P. S. *J. Med. Chem.* **2010**, *53*, 6811−6824.
(50) Deria, P.; Mondloch, J. E.; Tylianakis, E.; Ghosh, P.; Bury, W.; Snurr, R. Q.; Hupp, J. T.; Farha, O. K. *J. Am. Chem. Soc.* **2013**, *135*, 16801−16804.
(51) Masters, J. R. *Nat. Rev. Cancer.* **2002**, *2*, 315−319.
(52) Kim, J.; Tung, C.-H.; Choi, Y. *Chem. Commun.* **2014**, *50*, 10600−10603.
(53) Jhung, S. H.; Lee, J.-H.; Yoon, J. W.; Serre, C.; Férey, G.; Chang, J.-S. *Adv. Mater.* **2007**, *19*, 121−124.
(54) Carné-Sánchez, A.; Imaz, I.; Cano-Sarabia, M.; Maspoch, D. *Nat. Chem.* **2013**, *5*, 203−211.

DOI: 10.1021/jacs.6b00007
J. Am. Chem. Soc. 2016, 138, 3518−3525